# Integration of Quantum Cascade Lasers and Passive Waveguides[a]

Juan Montoya,[1, b] Christine Wang,[1] Anish Goyal,[1] Kevin Creedon,[1] Michael Connors,[1] Jeffrey Daulton,[1] Joseph Donnelly,[1] Leo Missaggia,[1] Chris Aleshire,[1] Antonio Sanchez-Rubio,[1] and William Herzog[1]

*MIT Lincoln Laboratory, 244 Wood St, Lexington, MA. 02420*

(Dated: 1 June 2015)

We report on monolithic integration of active quantum cascade laser (QCL) materials with passive waveguides formed by using proton implantation. Proton implantation reduces the electron concentration in the QCL layers by creating deep levels that trap carriers. This strongly reduces the intersubband absorption and the free-carrier absorption in the gain region and surrounding layers, thus significantly reducing optical loss. We have measured loss as low as $\alpha = 0.33\ cm^{-1}$ in $\lambda = 9.6\ \mu m$ wavelength proton-implanted QCL material. We have also demonstrated lasing in active-passive integrated waveguides. This simple integration technique is anticipated to enable low-cost fabrication in infrared photonic integrated circuits (PICs) in the mid-infrared ($\lambda \sim 3 - 16\ \mu$m).

Photonic integrated circuits (PICs) enable the monolithic integration of a variety of components such as lasers, amplifiers, detectors, wavelength combiners, power splitters, and so forth. Some interesting applications such as remote sensing, spectroscopy[1], and phased-array ladar[2] benefit from scaling the output power of quantum cascade lasers using coherent[3] or wavelength beam combining[4]. For these and other applications, integrating the active gain material with the relevant photonic elements monolithically on a common substrate requires passive elements having low optical loss.

Free-carrier and intersubband transition waveguide losses in QCLs may be as large[5] as $\alpha_w \sim 14\ cm^{-1}$ at wavelengths of $\sim 9\ \mu$m. Therefore, techniques must be developed to reduce the inherent losses in the active ma-
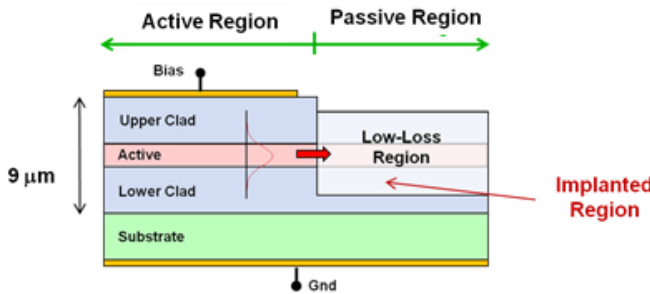


FIG. 1. Infrared active-passive integration concept: A section of a quantum cascade laser waveguide is selectively proton implanted to reduce the free-carrier and intersubband transition loss.

terial for realization of low-loss optical elements. One approach to achieving low loss is to selectively etch and regrow semi-insulating materials. This is particularly challenging in the infrared where the waveguide thickness approaches several microns. Moreover, the regrown passive waveguides must be aligned to the active waveguides to achieve good mode matching to avoid coupling loss.

Here we demonstrate for the first time, an alternate approach as shown in Fig.1 which utilizes proton implantation[6]. In this approach, the passive waveguide is selectively proton implanted to achieve low optical loss. This self-aligning approach achieves good mode matching as the active and passive waveguides may be defined in a single patterning step. Following patterning, metal contacts are made on the active section, and the active section quantum cascade laser material is biased to achieve gain.

Proton $(H^+)$ implantation reduces the free-carrier concentration and intersubband absorption by creating electron traps in the material. Previously, proton implantation was used to electrically isolate and control the current path through QCLs[7–9]. Additional consequences of proton implantation are to strongly reduce intersubband and free-carrier absorption in the QCL gain region and surrounding waveguide layers. In this work, we demonstrate proton-implanted QCL waveguides with reduced optical loss and the first monolithically integrated active QCL and passive waveguide using this approach.

The QCL structure was based on a GaInAs/AlInAs broadband bound-to-continuum heterostructure design[5] and was grown by organometallic vapor phase epitaxy on an n-type InP substrate[10]. A 3.5-$\mu$m-thick Si-InP (n $= 1 \times 10^{17}$ cm$^{-3}$) lower cladding is followed by a 0.52 $\mu$m thick layer of GaInAs (n $= 3 \times 10^{16}$cm$^{-3}$) waveguide, 35-period active region[5], 0.52 $\mu$m of GaInAs (n $= 3 \times 10^{16}$cm$^{-3}$) upper waveguide, 3.5 $\mu$m Si-InP (n $= 1 \times 10^{17}$cm$^{-3}$) upper cladding, 0.5 $\mu$m Si-InP (n $= 5 \times 10^{18}$cm$^{-3}$) plasmon layer, and 20 nm Si-GaInAs (n $= 1.8 \times 10^{19}$cm$^{-3}$) contact layer. No attempt was made to re-

duce the carrier concentration below typical QCL doping levels. The QCL lased at $\lambda \sim 9.6$ $\mu$m[11,12].

The QCL materials were proton implanted to sufficiently compensate the intentionally doped QCL materials. A model[13] was implemented to estimate the free-carrier loss as a result of the proton ($H^+$) implants. The carrier concentration is given by $n_0 = N_c e^{-(E_c-E_f)/kT}$ where $N_c$ relates to the density of states in the conduction band ($N_c \sim 6 \times 10^{17}$ cm$^{-3}$ in InP), $E_c$ is the conduction band energy, $E_f$ is the Fermi level energy, and $kT$ is the product of the Boltzmann constant and temperature. The proton implants create trap energies that reside $\sim$ 0.2-0.3 eV below the conduction band edge in InP[13]. In the high-dose limit, which we assume is the case here, we assume that the Fermi level is pinned to the trap energy level. This is expected to result in a residual free-carrier concentration of $n_0 \sim 10^{14}$ cm$^{-3}$ after implantation, and below our target level of $10^{15}$ cm$^{-3}$, which we anticipate to result in an optical loss of $\alpha < 0.1$ cm$^{-1}$. The loss in each waveguide layer is assumed to scale as $\alpha_i = 0.7$ cm$^{-1} \times \frac{n}{(10^{16})} (\frac{\lambda}{10\mu m})^r$, where the loss value at $\lambda = 10$ $\mu$m is estimated from the reported literature values[14] based on loss measuurements in InP as a function of carrier-concentration $n$ . The free-carrier loss scales[15] with a $\lambda^r$ dependence where the exponent $r$ depends on the dominant scattering mechanism and varies from 1.5 to 3.5. Alternate loss estimates may be arrived at assuming a classical Drude model and wavelength scaling with a $\lambda^2$ dependence.

A proton implant schedule using a software package SRIM[16] was designed to achieve a uniform proton concentration of $\sim 10^{17}$ cm$^{-3}$ to compensate the doped QCL layers. The schedule used energies from 100-800 keV with dose variations ranging from from 2 to $6 \times 10^{13}$ cm$^{-2}$.

Both passive waveguides and integrated active and passive waveguide structures were fabricated. For passive waveguides, ridges 12 $\mu$m wide and 3 mm long were first fabricated and then proton implanted. For the monolithically integrated active and passive waveguide structure, the passive waveguide material was first proton implanted, and then ridges were fabricated.

Loss measurement were performed by using a mode-hop free tunable QCL ($\lambda \sim 9.6$ $\mu$m). Figure 2 shows the transmission through a 3.0 mm long, 12 $\mu$m wide ridge, proton-implanted waveguide. The resulting transmission curve is illustrated in Fig. 2. Also shown in Fig. 2 is the transmission for an unimplanted sample. From the implanted data we estimate a free-spectral range (FSR) $\sim$ 0.49 cm$^{-1}$ from which we estimate a group index $n_g \sim 3.4$. We note that the group index is always larger then the modal index in this material and is in good agreement with reported values for similar structures[17]. The contrast $\gamma$ of the interference fringes observed in transmission is defined as $\gamma = \frac{P_{max}-P_{min}}{P_{max}+P_{min}}$, where $P_{max}$ and $P_{min}$ are the maximum and minimum of the inteference fringes respectively. From the measured data shown in Fig. 2, we estimate a contrast $\gamma = 0.47$. Using this contrast, we can estimate the waveguide loss $\alpha_w$ by the following expression[18]

$$\alpha_w = -\frac{1}{L} \ln(\frac{1 - \sqrt{(1 - \gamma^2)}}{\gamma R}). \qquad (1)$$

In the loss expression, the facet reflectivity is related to the surrounding index $n_0 = 1$ and the waveguide modal index $n_{eff} \sim 3.2$ by $R = (\frac{n_0 - n_{eff}}{n_0 + n_{eff}})^2 \sim 0.27$. Using this value for $R$ we estimate a loss of $\alpha = 0.33$ cm$^{-1}$ for our L=3.0 mm wet-etched waveguide at a $\lambda = 9.6$ $\mu$m wavelength. The transmission through the unimplanted sample is also shown in Figure 3 for comparison. We note that the contrast is degraded as anticipated for larger losses. From the unimplanted data, we estimate the contrast to be less than 7 percent with large uncertainty due to the signal to noise ratio in the data. Inserting this contrast into the loss expression in Eq. 1, we estimate the loss to be greater than 7 cm$^{-1}$.

Given the large uncertainty in the fringe-contrast measurement for large loss ($\alpha L \sim 1$)[18], we have turned to alternate methods based on observation of the threshold dependence on cavity length to provide a better estimate of the waveguide loss. The current density threshold dependence in a QCL may be expressed in terms of a mirror loss $\alpha_m$ and waveguide loss $\alpha_w$ as in

$$J_{th} = \frac{\alpha_m + \alpha_w}{g\Gamma}, \qquad (2)$$

where $g$ is a differential gain , $\Gamma$ is the confinement factor, and the mirror loss[5] is given by $\alpha_m = \frac{1}{L} \ln R$.

Shown in Fig. 3 is the power as a function of current measured from a QCL cut-back to different lengths (L=3.0 mm and L=5.0 mm) taken under pulsed conditions (200 ns pulses with a 0.02 percent duty cycle). We can use the threshold current density relation expressed in Eq. 2 to solve for the waveguide loss $\alpha_w$ as we vary the mirror loss by varying the waveguide length for our assumed reflectivity $R$. We note that the current threshold may be related to the current density ($I_{th} = J_{th} w_{eff} L$) where $w_{eff}$ is an effective ridge width. Furthermore, to solve for the waveguide loss it is convenient to express $\alpha_w$ in terms of a ratio of threshold measurements ($\beta = \frac{J_{th,L_1} - J_{th,L_2}}{J_{th,L_1}}$) for cavity lengths $L_1$ and $L_2$ in order to cancel common terms $\gamma, w_{eff}, g$ which are not needed to solve for $\alpha_w$. In doing so, we find $\alpha_w = 12.3$ cm$^{-1}$. We note that this loss value compares favorably with reported loss values of 14 cm$^{-1}$ in the literature[5].

In an effort to fully demonstrate the utility of the passivation technique we have integrated an active and passive waveguide. A microscope image of a typical integrated waveguide is shown in Fig 4. The fabrication of the integrated active and passive waveguide structure is described as follows: A thin silicon nitride film was blanket deposited onto the grown structure. A 7 $\mu$m thick silver film was deposited and used to selectively mask the active region. A software package SRIM was used to determine the silver film thickness required to protect
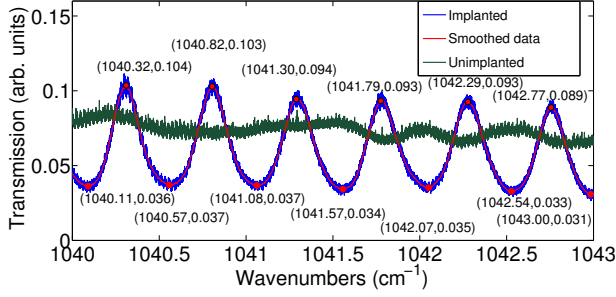
FIG. 2. Transmission through a 3 mm (blue) proton-implanted and (green) unimplanted QCL waveguide as a function of wavelength. A FSR of $\sim 0.49$ cm$^{-1}$ was inferred from the data. The fringe contrast of the implanted waveguide was measured to be 47 percent consistent with a loss of $\alpha_w = 0.33$ cm$^{-1}$. The unimplanted sample resulted in a fringe contrast $< 7$ percent consistent with a loss $\alpha > 7$ cm$^{-1}$.
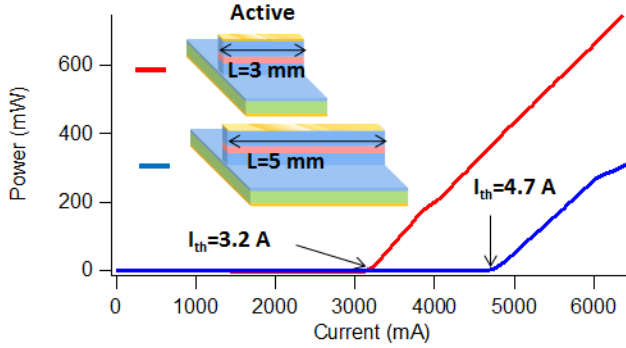


FIG. 3. Power versus current (LI) data measured from a QCL laser of different lengths used to extract the waveguide loss. LI curves are shown for a (red) 3 mm long active waveguide and a (blue) 5 mm long active waveguide.

the active region from the most energetic protons. The sample was subsequently proton implanted. The implant mask was then removed using a standard wet-etch process. The 12 $\mu$m wide ridge waveguides were then patterned and contacts were formed in the active region. We note that the contact metal was recessed approximately 20 $\mu$m from the active-passive junction to accommodate any straggle (lateral spreading) of the proton implants. It should also be noted that a process was used to prevent the temperature from rising beyond 70 °C to prevent the implantation-induced traps from being annealed, and thus increasing the loss in the passive region[19].

The threshold condition in an active-passive waveguide may be derived under the constraint that the gain compensates for the cavity losses which may be expressed as $1 = Re^{(g_A L_A - \alpha_A L_A - \alpha_P L_P)}$, where $L_A$ is the length of the active region with gain $g_A$, and $L_P$ is the length of the passive region with loss $\alpha_P$. For convenience, we can define an effective mirror loss $e^{\alpha_m L_A} = R$ referenced to the active region such that $\alpha_m = \frac{\ln(R)}{L_A}$. This definition allows us to modify Eq. 2 to take into account the passive

waveguide section as expressed below:

$$J_{th} = \frac{\alpha_m + \alpha_A + \alpha_P \frac{L_P}{L_A}}{g\Gamma}. \qquad (3)$$

We note that Eq. 3 reverts to Eq. 2 in the limit that $L_P = 0$. Having a measured $\alpha_A$, and assumed $\alpha_m$, we can solve Eq. 3 for $\alpha_P$ simply by varying the passive waveguide length $L_P$ and observing the change in threshold. Following a similar development to the active-only threshold measurements, we can define a ratio $\chi = \frac{J_{th,L_p} - J_{th,0}}{J_{th,0}} = \frac{I_{th,L_P} - I_{th,0}}{I_{th,0}}$ where the subscripts $(L_p, 0)$ denote an active-passive waveguide with passive length of $L_p$ and 0 respectively. With the aid of Eq. 3, we find $\chi = \frac{\alpha_P \frac{L_A}{L_P}}{\alpha_A + \alpha_M}$. In order to calculate the threshold ratio $\chi$, LI measurements were made as the passive waveguide was cleaved to three different lengths: $L_P = 5$ mm, $L_P = 3$ mm, and $L_P = 0$ mm as shown in Fig. 5. From the measurements shown in Fig. 5 we extract a threshold ratio $\chi = 0.1$. Using our assumed mirror loss $\alpha_m = 4.4$ cm$^{-1}$, and measured active waveguide loss $\alpha_A = 12.3$ cm$^{-1}$, we find $\alpha_P = 1.7$ cm$^{-1}$.

The observed threshold behavior as the passive waveguide is varied therefore demonstrates that ion implantation may be used to significantly reduce the loss of a QCL waveguide from an initial value of $\alpha_A = 12.3$ cm$^{-1}$ to a lower value of $\alpha_P = 1.7$ cm$^{-1}$ after passivation. While the 1.7 cm$^{-1}$ loss in the passive section of the active-passive integrated waveguide was notably higher than the 0.3 cm$^{-1}$ loss measured in a passive-only waveguide (i.e. not integrated with an active-waveguide), the discrepancy may partially be accounted for in the difference in fabrication. The passive-only waveguide structure had been patterned first and subsequently implanted whereas the active-passive had been initially implanted and then patterned at a lower process temperature. Furthermore, the active-passive waveguide also contained a junction between waveguides in which the metal was re-
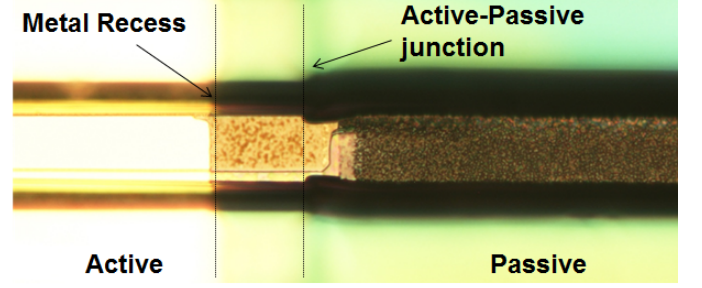


FIG. 4. Microscope image of an integrated active and passive waveguide. A transition region is shown between the active and passive waveguides as a result of the microfabrication processing of two regions with different thicknesses. The metal was recessed to accommodate lateral spreading of the protons.
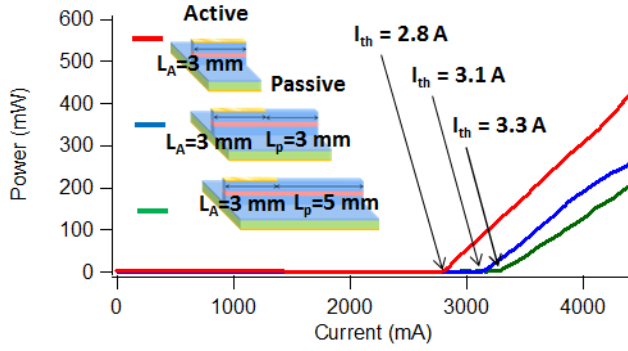
FIG. 5. Power versus current (LI) data measured from a QCL active waveguide integrated with a passive waveguide cut-back to different lengths. Measurements are shown for a 3 mm active section and passive waveguide section lengths L=(5 mm, 3 mm, 0 mm) with corresponding thresholds $I_{th}$=(3.3 A, 3.1 A, 2.8 A) respectively.

cessed within the active region which may also have contributed to larger losses. Achieving higher yield in the active-passive integrated structures along with an improvement in microfabrication, particularly at the junction of the active-passive waveguide, may allow us to bridge the gap and achieve losses as low as 0.3 cm$^{-1}$ in integrated active-passive waveguide structures.

In conclusion, we have demonstrated reduced optical loss using proton implantation. We have measured losses as low as $\alpha_w = 0.3$ cm$^{-1}$ in passive (unbiased) proton-implanted QCL waveguides. We have further demonstrated integration of an active and passive waveguide, and lasing through a 5 mm passive waveguide section with losses $\alpha_P = 1.7$ cm$^{-1}$. This low cost passivation technique shows promise toward enabling infrared photonic integrated circuits and several compelling applications such as monolithic beam combining, optical phased array ladar, and remote sensing.

[1] A. Soibel, K. Mansour, S. Forouhar, M. L. Peabody, D. L. Sivco, A. Y. Cho, and C. Gmachl, in *Lasers and Electro-Optics, 2005. (CLEO). Conference on*, Vol. 2 (2005) pp. 863–865.

[2] J. Montoya, A. Sanchez-Rubio, R. Hatch, and H. Payson, Appl. Opt. **53**, 7551 (2014).

[3] J. Montoya, S. J. Augst, K. Creedon, J. Kansky, T. Y. Fan, and A. Sanchez-Rubio, Appl. Opt. **51**, 1724 (2012).

[4] A. K. Goyal, M. Spencer, O. Shatrovoy, B. G. Lee, L. Diehl, C. Pfluegl, A. Sanchez, and F. Capasso, Opt. Express **19**, 26725 (2011).

[5] A. Wittmann, T. Gresch, E. Gini, L. Hvozdara, N. Hoyler, M. Giovannini, and J. Faist, IEEE J. Quantum Electron. **44**, 36 (2008).

[6] A. Goyal, L. Diehl, C. Pfluegl, C. Wang, and M. Witinski, "Photonic integrated circuits based on quantum cascade structures," (2014), uS Patent App. 13/951,240.

[7] H. Page, S. Dhillon, M. Calligaro, V. Ortiz, and C. Sirtori, Electron. Lett. **39**, 1053 (2003).

[8] M. Semtsiv, S. Dressler, U. Muller, S. Knigge, M. Ziegler, and W. Masselink, IEEE J. Quantum Electron. **42**, 490 (2006).

[9] C. Faugeras, S. Forget, E. Boer-Duchemin, H. Page, J.-Y. Bengloan, O. Parillaud, M. Calligaro, C. Sirtori, M. Giovannini, and J. Faist, IEEE J. Quantum Electron. **41**, 1430 (2005).

[10] C. Wang, R. Huang, A. Goyal, J. Donnelly, D. Calawa, S. Cann, F. ODonnell, J. Plant, L. Missaggia, G. Turner, and A. Sanchez-Rubio, J. Cryst. Growth **310**, 5191 (2008).

[11] P. Rauter, S. Menzel, B. Gokden, A. K. Goyal, C. A. Wang, A. Sanchez, G. Turner, and F. Capasso, Appl. Phys. Lett. **102**, 181102 (2013).

[12] P. Rauter, S. Menzel, A. K. Goyal, B. Gokden, C. A. Wang, A. Sanchez, G. W. Turner, and F. Capasso, Appl. Phys. Lett. **101**, 261117 (2012).

[13] J. Donnelly and C. Hurwitz, Solid-State Electron. **20**, 727 (1977).

[14] W. Walukiewicz, J. Lagowski, L. Jastrzebski, P. Rava, M. Lichtensteiger, C. Gatos, and H. Gatos, J. Appl. Phys. **51**, 2659 (1980).

[15] O. Kim and W. Bonner, J. Electron. Mater. **12**, 827 (1983).

[16] J. Ziegler, SRIM code, http://www.srim.org (2014).

[17] Q. Yang, M. Kinzer, R. Aidam, R. Driad, W. Bronner, S. Hugger, R. Ostendorf, F. Fuchs, and J. Wagner, J. Appl. Phys. **112**, 103109 (2012).

[18] D. F. Clark and M. S. Iqbal, Opt. Lett. **15**, 1291 (1990).

[19] S. J. Pearton, C. R. Abernathy, M. B. Panish, R. A. Hamm, and L. M. Lunardi, J. Appl. Phys. **66**, 656 (1989).

[20] C. Sirtori, J. Faist, F. Capasso, D. Sivco, A. Hutchinson, and A. Cho, Photonics Technology Letters, IEEE **9**, 294 (1997).

[21] K. Pierscinski, D. Pierscinska, M. Iwinska, K. Kosiel, A. Szerling, P. Karbownik, and M. Bugajski, J. Appl. Phys. **112**, 043112 (2012).